

Sources and Emission Time Scales in $E/A = 50$ MeV $^{129}\text{Xe} + ^{\text{nat}}\text{Cu}$ Reactions

D. R. Bowman,^(a) G. F. Peaslee, N. Carlin,^(b) R. T. de Souza,^(c) C. K. Gelbke, W. G. Gong,^(d) Y. D. Kim,^(e)
 M. A. Lisa, W. G. Lynch, L. Phair, M. B. Tsang, and C. Williams
*National Superconducting Cyclotron Laboratory and Department of Physics and Astronomy,
 Michigan State University, East Lansing, Michigan 48824*

N. Colonna,^(f) K. Hanold, M. A. McMahan, G. J. Wozniak, and L. G. Moretto
*Nuclear Science Division and Accelerator and Fusion Research Division,
 Lawrence Berkeley Laboratory, Berkeley, California 94720*

(Received 7 December 1992)

Velocity distributions and fragment-fragment correlation functions have been measured as a function of charged particle multiplicity for $^{129}\text{Xe} + ^{\text{nat}}\text{Cu}$ collisions at $E/A = 50$ MeV. With increasing multiplicity, the velocity distributions evolve from a pattern exhibiting targetlike and projectilelike sources to an anisotropic distribution centered near the projectile-target center-of-mass velocity. Emission times extracted from the correlation functions are consistent with the decay of a projectilelike source in low multiplicity collisions, but the time scale for fragment emission in the high multiplicity collisions is too short for a separation of sources to occur.

PACS numbers: 25.70.Pq

Recent experiments have demonstrated that nuclear systems undergo a multifragment disassembly following heavy ion reactions at both high [1–3] and intermediate bombarding energies [4–12]. The breakup mechanism has been associated with volume instabilities [13,14], which are related to a liquid-gas phase transition in nuclear matter [15], with a series of statistical binary decays [16–19], or with surface instabilities which can arise if nuclear systems attain exotic shapes [20,21]. For each of these proposed mechanisms fragment emission occurs on a characteristic time scale. It is important to characterize the source or sources of the multifragment disassembly and to determine the emission time scales experimentally. Information about the sources of emission can be obtained by measuring velocity distributions; for example, the observation of isotropic rings in velocity space has been given as vivid evidence for a source decaying via a binary mechanism [10,16]. However, these distributions cannot give quantitative information about the time scale of fragment emission. Fragment-fragment correlation functions are more suited to providing information about emission time scales [22–26].

Studies of fragment-fragment correlations have indicated fragment emission time scales ≤ 100 – 200 fm/c, consistent with fast, nonsequential breakup processes [23–25]. In these measurements, central collisions were selected by multiplicity cuts, but no detailed information about the distribution of fragments in velocity space was obtained. In this paper, for the first time, we characterize the sources of fragment emission in both central and peripheral collisions by measuring fragment velocity distributions, and experimentally determine the time scales associated with fragment emission from these sources.

The experiment was performed using the K1200 Cyclotron at the National Superconducting Cyclotron Laboratory at Michigan State University (MSU). A beam

of ^{129}Xe ions with intensity $\sim 10^7$ particles/s impinged upon $^{\text{nat}}\text{Cu}$ targets of thickness 2 mg/cm². Intermediate mass fragments and light charged particles were detected at angles of 16° – 160° using the MSU Miniball phoswich array [27], which covered approximately 87% of 4π . At more forward angles, 2° – 16° , sixteen position-sensitive Si-Si(Li)-plastic telescopes were placed [28]. The energy calibrations are estimated to be accurate to 1% for fragments stopped in the Si(Li) detectors and (5–10)% for fragments and particles detected with the Miniball. The position resolution of the Si telescopes is approximately ± 1.5 mm in both the X and Y dimensions. Additional experimental details are given in Ref. [12].

Figure 1 shows the cross sections in velocity space for $Z = 2$ and $Z = 6$ fragments with two different gates on the total charged particle multiplicity, N_C . The limits of the detector acceptance are indicated by the solid lines in the figure. In order to obtain continuous distributions, the yields at angles $>16^\circ$ have been randomized over the face of the struck Miniball detector.

Peripheral collisions (left hand panels) show one component centered at a parallel velocity slightly less than that of the beam (indicated by the black arrows in the left hand panels) and another component centered at a parallel velocity slightly larger than zero. We interpret these components as due to the decay of projectilelike (PLF) and targetlike fragments (TLF). These fragments are not completely equilibrated since the emission is preferentially backward in the frame of the PLF, and preferentially forward in the frame of the TLF, which leads to enhanced fragment yields at intermediate velocities. This enhancement is particularly evident for the $Z = 6$ fragments. Fits of such velocity distributions require emission from three (isotropic) sources: a PLF, a TLF, and a third “nonequilibrium” source with a velocity approximately one-half of that of the beam (nucleon-nucleon

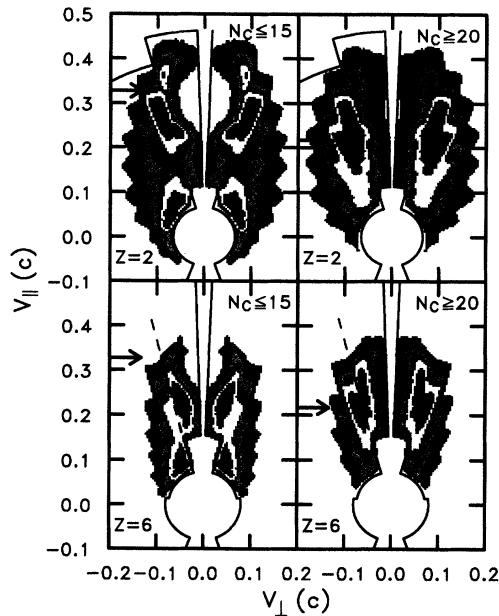


FIG. 1. Linear density plots of $d^2\sigma/dv_{\parallel}dv_{\perp}$ for $Z = 2$ (top panels) and $Z = 6$ (bottom panels) fragments. Distributions gated on low (high) charged particle multiplicity, N_C , are shown in the left (right) panels. Regions of red, yellow, green, blue, and purple correspond to relative yields of 5, 4, 3, 2, and 1, respectively. The limits of the (Si) detector acceptance are indicated by the solid (dashed) lines. The arrows in the left (right) panels indicate the beam (center-of-mass) velocity.

center-of-mass frame) [24,29].

The right-hand panels in Fig. 1 show velocity distributions for $Z = 2$ and $Z = 6$ fragments gated on high multiplicity collisions. These distributions are broad, anisotropic, and centered at approximately the projectile-target center-of-mass velocity (black arrows on the right-hand panels).

In order to obtain quantitative information about the time scales of fragment emission we have constructed two-fragment, velocity correlation functions defined as

$$\sum Y_{12}(\mathbf{v}_1, \mathbf{v}_2) = C[1 + R(v_{\text{red}})] \sum Y_1(\mathbf{v}_1)Y_2(\mathbf{v}_2),$$

where \mathbf{v}_1 and \mathbf{v}_2 are the laboratory velocities of the fragments, v_{red} is the reduced relative velocity, $v_{\text{red}} = (\mathbf{v}_1 - \mathbf{v}_2)/\sqrt{Z_1 + Z_2}$, and C is a normalization constant determined by requiring $R(v_{\text{red}}) \approx 0$ at large relative velocities where the final state interaction is small. The singles yields, Y_1 and Y_2 , are taken from the same events as the coincidence yield, Y_{12} . The reduced relative velocity, v_{red} , is introduced to eliminate the charge dependence of the relative fragment velocity in mixed fragment correlation functions [24,30]. We have verified with $Z_1 = Z_2$ correlation functions that there is little dependence of v_{red} on Z for $v_{\text{red}} > 0.01c$.

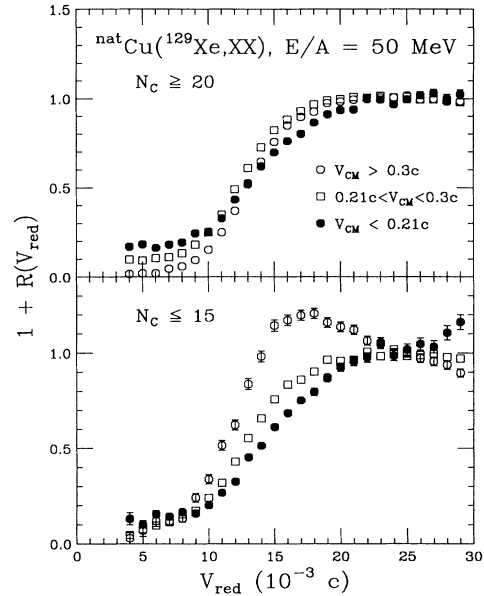


FIG. 2. Experimental correlation functions for $5 \leq Z_1, Z_2 \leq 12$ fragments as a function of the reduced relative velocity, v_{red} . The top (bottom) panel corresponds to high (low) multiplicity events. The solid circles, open circles, and open squares correspond to events gated on the indicated ranges of center-of-mass velocity of the two fragments.

In Fig. 2, we show mixed fragment correlation functions ($5 \leq Z_1, Z_2 \leq 12$) for fragments stopped in the Si(Li) detectors. The limits of acceptance of these detectors ($2^\circ < \theta_1, \theta_2 < 16^\circ$) are shown by the dashed lines in the bottom panels of Fig. 1. The top and bottom panels of Fig. 2 show correlation functions gated on high and low multiplicity, respectively, for three gates on the center-of-mass (c.m.) velocity of the two fragments. While there are quantitative differences in the high multiplicity correlation functions, the shapes of the curves are similar. In contrast, the correlation functions gated on low multiplicity collisions exhibit dramatic differences in shape. For $V_{\text{c.m.}} > 0.3c$ there is a maximum at $v_{\text{red}} = 0.017c$, which is absent in all other correlation functions. Correlation functions which do not tend asymptotically to 1.0 for $v_{\text{red}} > 0.015c$ were previously observed [25,26], and interpreted [25] as due to three-body effects.

Let us first consider the peripheral reactions [31]. The correlation functions in the bottom panel of Fig. 2 appear to indicate shorter emission time scales for fragments with $V_{\text{c.m.}} < 0.3c$ than for fragments with $V_{\text{c.m.}} > 0.3c$. Such a trend is expected since nonequilibrium contributions are important at intermediate velocity [32]. However, a combination of sources gives rise to correlation functions which are difficult to interpret [33]. Therefore we will quantify the fragment emission time scale only for fragment pairs with a c.m. velocity $> 0.3c$, for which contributions from the projectilelike source are enhanced (see Fig. 1).

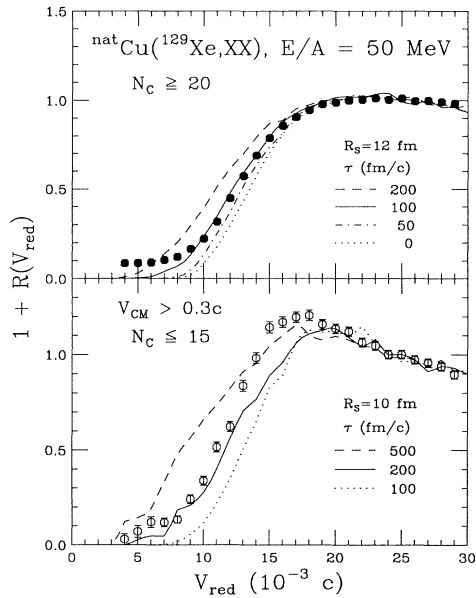


FIG. 3. Comparison of experimental correlation functions (solid and open points) with three-body trajectory calculations (curves). The top panel shows results gated on high multiplicity events, and the bottom panel results gated on low multiplicity events for fragments with a center-of-mass velocity $> 0.3c$. The curves correspond to calculations with the indicated source radii, R_S , and mean emission times, τ .

Simulated events from a three-body trajectory calculation [23,24,30] were generated using the experimental charge, energy, and angular distributions, subsequently filtered through a software replica of the experimental apparatus, and analyzed in the same manner as the experimental data. The calculated correlation functions are sensitive to the space-time extent of the emitting source. In the simulations we have fixed the source radius, R_S , at 10 fm and the total charge, mass, and velocity of the system at 54, 129, and $0.33c$, respectively, equal to the projectile charge, mass, and velocity. In the bottom panel of Fig. 3, the simulated correlation function with mean emission times, τ , of 100, 200, and 500 fm/c are compared with the experimental data; a mean emission time of 200 fm/c gives the best agreement [34]. We have performed other calculations with identical emission times and $R_S = 8$ and 12 fm [35]. To quantify the agreement between the simulations and the experimental data, the reduced χ^2 values are presented in Table I [36]. For any reasonable choice of radius parameter, the time scale for emission of high velocity fragments in peripheral reactions is on the order of 200–500 fm/c.

Now let us consider the central reactions. We have not placed a gate on c.m. velocity due to the single apparent source observed in the velocity distributions and the similarity of the velocity gated correlation functions shown in the upper panel of Fig. 2. For these simulations we have chosen a source charge, mass, and velocity of 83,

TABLE I. Reduced χ^2 values, χ^2/ν , for calculated correlation functions for fragment pairs with $V_{c.m.} > 0.3c$ in low multiplicity collisions.

| τ (fm/c) | R_S (fm) | | |
|---------------|------------|------|------|
| | 8 | 10 | 12 |
| 500 | 8.3 | 14.5 | 19.4 |
| 200 | 8.8 | 8.2 | 4.8 |
| 100 | 76.7 | 49.5 | 24.8 |

193, and 0.22, respectively, corresponding to complete fusion of projectile and target. In the top panel of Fig. 3 the experimental data for high multiplicity collisions are compared with three-body trajectory calculations with $R_S = 12$ fm and $\tau = 0, 50, 100$, and 200 fm/c. The data show best agreement with the simulation for $\tau = 100$ fm/c. In Table II, the reduced χ^2 values for these simulations, along with others for identical mean emission times and $R_S = 10$ and 14 fm [35] are shown [36]. For any reasonable choice of radius parameter, the time scale for fragment emission in central collisions is ≤ 100 fm/c. These time scales are consistent with those extracted for central collisions in $^{36}\text{Ar} + ^{197}\text{Au}$ reactions at $E/A = 35$ –110 MeV [23–25].

We have varied the source velocity and source charge parameters to investigate the uncertainties in the results of the three-body simulations. The source velocity was varied between the nucleon-nucleon center-of-mass velocity ($0.16c$) and the beam velocity ($0.33c$). The source charge was varied between 0 and 83 (complete fusion). The sensitivity of the calculations to these parameters corresponds to an uncertainty in mean emission time of ≈ 50 fm/c.

The fragment velocity distributions shown in Fig. 1 indicate emission time scales for peripheral collisions long enough to allow the separation of the PLF and TLF, as predicted by the deep inelastic scattering and incomplete fusion mechanisms, but shorter than the rotational time of the excited PLF. Assuming a relative velocity equal to the beam velocity, the time required for the ^{129}Xe projectile to pass the ^{nat}Cu target is ≈ 70 fm/c. This time is a lower limit to the projectile-target separation time; any dissipation of the entrance channel kinetic energy will give a longer separation time. The time necessary for rotation of a ^{129}Xe nucleus with angular momentum of $J = 88\hbar$ [37] is approximately 700 fm/c (smaller val-

TABLE II. Reduced χ^2 values, χ^2/ν , for calculated correlation functions in high multiplicity collisions.

| τ (fm/c) | R_S (fm) | | |
|---------------|------------|-------|-------|
| | 10 | 12 | 14 |
| 200 | 54.3 | 83.7 | 106.1 |
| 100 | 7.0 | 3.5 | 23.1 |
| 50 | 177.4 | 32.3 | 3.8 |
| 0 | 704.5 | 147.5 | 26.6 |

ues of J will lead to correspondingly longer rotational times). As expected, the emission time of 200–500 fm/ c extracted for high velocity fragments in peripheral collisions falls between the PLF-TLF separation time and the PLF rotational time.

The emission time scale of ≤ 100 fm/ c extracted for central collisions is similar to the separation time of the PLF and TLF calculated above. This short time scale precludes PLF/TLF mechanisms such as deep inelastic scattering or incomplete fusion and accounts for the single apparent source in the observed velocity distributions.

In summary, we have compared fragment velocity distributions and fragment-fragment correlation functions for the $^{129}\text{Xe} + \text{natCu}$ reaction at $E/A = 50$ MeV. In peripheral collisions a projectilelike source exists which decays on a time scale long enough to allow separation from a targetlike fragment, but of insufficient lifetime to allow complete equilibration. Central collisions are characterized by broad, anisotropic velocity distributions and decay times too short to allow a separation of sources.

Fruitful discussions with Scott Pratt are gratefully acknowledged. This work was supported by the National Science Foundation under Grant No. PHY-89-13815 and the U.S. Department of Energy under Contract No. DE-AC03-76SF00098. W.G.L acknowledges support from the U.S. Presidential Young Investigator Program and N.C. acknowledges partial support by the FAPESP, Brazil.

(a) Present address: Chalk River Laboratories, Chalk River, Ontario, Canada K0J 1J0.

(b) Present address: Instituto de Física, Universidade de Sao Paulo, C. Postal 20516, CEP 01498, Sao Paulo, Brazil.

(c) Present address: Department of Chemistry and Indiana University Cyclotron Facility, Bloomington, IN 47405.

(d) Present address: Lawrence Berkeley Laboratory, Berkeley, CA 94720.

(e) Present address: Indiana University Cyclotron Facility, Bloomington, IN 47405.

(f) Present address: INFN - Sez. di Bari, 70126 Bari, Italy.

[1] J.W. Harris *et al.*, Nucl. Phys. **A471**, 241c (1987).

[2] C.A. Ogilvie *et al.*, Phys. Rev. Lett. **67**, 1214 (1991).

[3] J.P. Alard *et al.*, Phys. Rev. Lett. **69**, 889 (1992).

[4] Y.D. Kim *et al.*, Phys. Rev. Lett. **63**, 494 (1989).

[5] Y. Blumenfeld *et al.*, Phys. Rev. Lett. **66**, 576 (1991).

[6] E. Piasecki *et al.*, Phys. Rev. Lett. **66**, 1291 (1991).

[7] D.R. Bowman *et al.*, Phys. Rev. Lett. **67**, 1527 (1991).

[8] R.T. de Souza *et al.*, Phys. Lett. B **268**, 6 (1991).

[9] K. Hagel *et al.*, Phys. Rev. Lett. **68**, 2141 (1992).

[10] B. Lott *et al.*, Phys. Rev. Lett. **68**, 3141 (1992).

[11] T.C. Sangster *et al.*, Phys. Rev. C **46**, 1404 (1992).

[12] D.R. Bowman *et al.*, Phys. Rev. C **46**, 1834 (1992).

[13] J.P. Bondorf *et al.*, Nucl. Phys. **A443** 321 (1985); **A444**, 460 (1985).

[14] D.H.E. Gross *et al.*, Phys. Rev. Lett. **56**, 1544 (1986).

[15] P.J. Siemens, Nature (London) **305**, 410 (1983).

[16] L.G. Moretto and G.J. Wozniak, Prog. Part. Nucl. Phys. **21**, 401 (1988), and references therein.

[17] W.A. Friedman and W.G. Lynch, Phys. Rev. C **28**, 16 (1983).

[18] J. Richert and P. Wagner, Nucl. Phys. **A517**, 399 (1990).

[19] W.A. Friedman, Phys. Rev. Lett. **60**, 2125 (1988).

[20] L.G. Moretto *et al.*, Phys. Rev. Lett. **69**, 1884 (1992).

[21] W. Bauer *et al.*, Phys. Rev. Lett. **69**, 1888 (1992).

[22] R. Trockel *et al.*, Phys. Rev. Lett. **59**, 2844 (1987).

[23] Y.D. Kim *et al.*, Phys. Rev. Lett. **67**, 14 (1991).

[24] Y.D. Kim *et al.*, Phys. Rev. C **45**, 338 (1992).

[25] D. Fox *et al.*, Phys. Rev. C **47**, R421 (1993).

[26] T.C. Sangster *et al.*, Lawrence Livermore National Laboratory Report No. UCRL-JC-112127 (to be published).

[27] R.T. de Souza *et al.*, Nucl. Instrum. Methods Phys. Res., Sect. A **295**, 109 (1990).

[28] W.L. Kehoe *et al.*, Nucl. Instrum. Methods Phys. Res., Sect. A **311**, 258 (1992).

[29] B.V. Jacak *et al.*, Phys. Rev. C **35**, 1751 (1987).

[30] Y.D. Kim *et al.*, Phys. Rev. C **45**, 387 (1992).

[31] The distributions shown in Fig. 2 select peripheral collisions that are on average slightly more violent ($\langle N_c \rangle = 13$) than the events leading to $Z = 2$ ($\langle N_c \rangle = 10$) or $Z = 6$ ($\langle N_c \rangle = 11.5$) emission shown in Fig. 1. The velocity distributions gated on two-fragment events are qualitatively similar to those shown in Fig. 1. For central collisions, all of the distributions shown in Figs. 1 and 2 select events with approximately the same average multiplicity ($\langle N_c \rangle \approx 22$).

[32] W.G. Lynch, Annu. Rev. Nucl. Part. Sci. **37**, 493 (1987).

[33] S. Pratt (private communication).

[34] The theoretical and experimental correlation functions were normalized in the region $v_{\text{red}} > 0.022c$.

[35] For orientation, the distances between the centers of a ^{12}C fragment and the residues corresponding to a ^{129}Xe source (projectile) and a ^{193}Bi source (complete fusion) are 8.8 and 9.7 fm, respectively.

[36] The reduced χ^2 values were determined from the ascending portions of the correlation functions, $0.01c \leq v_{\text{red}} \leq 0.020c$ for high multiplicity events and $0.008c \leq v_{\text{red}} \leq 0.015c$ for low multiplicity events.

[37] The maximum angular momentum a ^{129}Xe nucleus can sustain with a nonzero fission barrier is $88\hbar$.

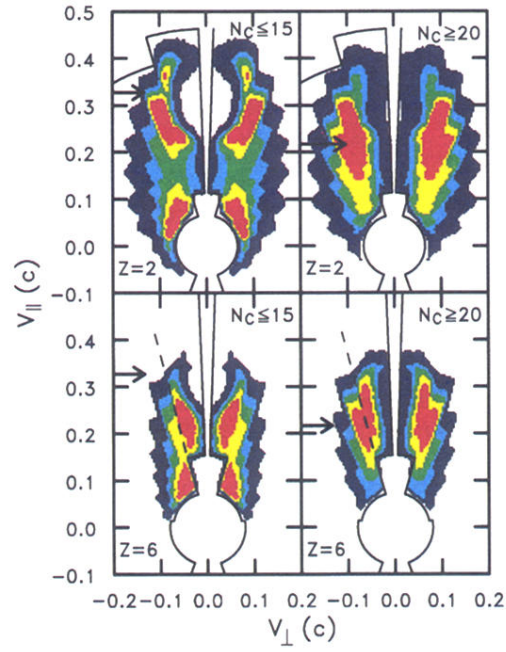


FIG. 1. Linear density plots of $d^2\sigma/dv_{\parallel}dv_{\perp}$ for $Z = 2$ (top panels) and $Z = 6$ (bottom panels) fragments. Distributions gated on low (high) charged particle multiplicity, N_C , are shown in the left (right) panels. Regions of red, yellow, green, blue, and purple correspond to relative yields of 5, 4, 3, 2, and 1, respectively. The limits of the (Si) detector acceptance are indicated by the solid (dashed) lines. The arrows in the left (right) panels indicate the beam (center-of-mass) velocity.